Available online at www.sciencedirect.com
ScienceDirect
Journal of the European Ceramic Society 27 (2007) 4479–4487
www.elsevier.com/locate/jeurceramsoc

Effect of glass additions on the sintering and microwave properties of composite dielectric ceramics based on $BaO–Ln_2O_3–TiO_2$ (Ln = Nd, La)

Hong Zheng [a,*], Ian M. Reaney [a], Duncan Muir [b], Tim Price [b], David M. Iddles [b]

[a] *Department of Engineering Materials, University of Sheffield, Sheffield S1 3JD, UK*
[b] *Filtronic Comtek, Ceramics Division, Wolverhampton WV10 7DB, UK*

Received 27 July 2006; received in revised form 16 March 2007; accepted 25 March 2007
Available online 6 June 2007

Abstract

Ten weight percent BBZS (Bi_2O_3, B_2O_3, ZnO and SiO_2) glass was added to $x(Ba_4Nd_{9.333}Ti_{18}O_{54}) - (1-x)(BaLa_4Ti_4O_{15})$ (BNLT, $0 \le x \le 1$) composite dielectric ceramics to lower their sintering temperature whilst retaining microwave properties useful for low temperature co-fired ceramic and antenna core technology. With the addition of 10 wt% BBZS glass, dense BNLT composite ceramics were produced at temperatures between 950 and 1140 °C, depending on composition (x), an average reduction of sintering temperature by 350 °C. X-ray diffraction, scanning and transmission electron microscopy and Raman spectroscopy studies revealed that there was limited inter-reaction between BLT/BNT and the BBZS glass. Microwave property measurement showed that the addition of BBZS glass to BNLT ceramics had a negligible effect on ε_r and τ_f, although deterioration in the measured quality factor (Qf) was observed. The optimised composition (xBNT $-(1-x)$BLT)/0.1BBZS ($x = 0.75$) had $\varepsilon_r \sim 61$, $\tau_f \sim 38$ ppm/°C and $Qf \sim 2305$ GHz.

Keywords: Dielectric ceramics; Low-melting glass addition

1. Introduction

Microwave (MW) dielectric ceramics are used in a range of thick film and bulk applications in the electronics industry, including NP0 chips (thick film), embedded capacitors (thick film) and dielectric resonators/filters (bulk). More recently, MW dielectric ceramics have been used as antenna cores (bulk) in global positioning systems and satellite radio handsets. Medium to high relative permittivities ($20 < \varepsilon_r < 80$), are generally required to miniaturise components but this cannot be done at the expense of decreasing the quality factor, Qf, below that required to select a narrow frequency range, where $Q \sim 1/\tan\delta$ and f is the resonant frequency. Additionally, components must be temperature stable with a temperature coefficient of the resonant frequency τ_f close to zero. The requirements for Qf and τ_f vary with the type of MW application. For bulk ceramics, the most stringent application is MW dielectrics for cavity filters and resonators, for which $Qf > 40{,}000$ GHz and $\tau_f = \pm 1$ ppm/°C. For antenna core technology, there is a less stringent requirement for Qf and τ_f since to some extent the contact metallisation dominates the dielectric loss broadening the resonant frequency. However, the vast array of different antenna frequencies requires materials with $20 < \varepsilon_r < 80$ since $f \propto 1/\sqrt{\varepsilon_r}$. In addition, the use of such materials in handsets will ultimately necessitate an extremely low raw material and processing cost as production volumes increase and profit margins reduce.

Our previous work[1] has successfully produced dielectric ceramics with a broad range of permittivities ($40 < \varepsilon_r < 78$) based on $xBa_4Nd_{9.333}Ti_{18}O_{54}$ (BNT) $-(1-x)BaLa_4Ti_4O_{15}$ (BLT) (BNLT, $0 \le x \le 1$) composites in which, $Qf \sim 10{,}000$ GHz and $-20 < \tau_f < 40$ ppm/°C. The Qf of these materials was considered too low for use as cavity resonators, but sufficient for thick film-based and antenna core applications. However, the high sintering temperature (≥1350 °C) precluded their use in co-fired thick film applications and also added to processing costs for the fabrication of antenna cores. This work therefore focuses on reducing the sintering temperature of the BNLT composite ceramics using low-melting glass.

Additions of low-melting glass have been widely used to reduce the sintering temperature in ceramics.[2–6] However, when

* Corresponding author.
E-mail address: hong.zheng@materials.ox.ac.uk (H. Zheng).

0955-2219/$ – see front matter © 2007 Elsevier Ltd. All rights reserved.
doi:10.1016/j.jeurceramsoc.2007.03.036

glass is used in microwave ceramics, *Qf* invariably deteriorates due to loss mechanisms associated with the glassy phase, such as resonance-type vibration losses at very high frequencies, migration losses caused by the movement of mobile ions, and deformation losses caused by distortion of the silicon oxide network.[7] Therefore, the selection of the glass is paramount in MW ceramics. Alumina-silicate-based glasses such as cordierite ($2MgO–Al_2O_3–SiO_2$) and celsian ($BaO–Al_2O_3–SiO_2$) have a high *Qf* at MW frequencies[8] but decrease the relative permittivity significantly. Recently, Dernovsek et al. have reported[3] that $BaO–Nd_2O_3–4TiO_2$ ceramics with varying additions of $B_2O_3–Bi_2O_3–ZnO–SiO_2$ (BBZS) are temperature stable with $20 < \varepsilon_r < 70$, when sintered at ~1000 °C. *Qf* varied across the compositional range but some samples achieved values >5000 GHz. BBZS was chosen by Dernovsek et al.[3] as a sintering aid because of its relatively high ε_r and *Qf* value (21 and 200 GHz, respectively) in the glass state and its low-meting point (<1000 °C).

The present study therefore concerns the effects of BBZS glass on the sintering behaviour and MW properties of BNLT composites. The shrinkage, phase assemblage and microstructures of the glass-containing BNLT composites are characterised using dilatometry, X-ray diffraction (XRD), scanning (SEM) and transmission (TEM) electron microscopy, energy-dispersive spectroscopy (EDS) and Raman spectroscopy.

2. Experimental

BBZS glass containing 35 mol% Bi_2O_3, 27 mol% B_2O_3, 32 mol% ZnO and 6 mol% SiO_2, as chosen by Dernovsek et al.,[3] was prepared by firing in platinum crucible at temperatures ~1000 °C. The BBZS glass frit was crushed, ground, and then ball milled to an average particle size of less than 6 μm. Ceramics of BNT and BLT were synthesized separately by a conventional mixed oxide route using $BaCO_3$, TiO_2, Nd_2O_3 and La_2O_3. The chemical purity of all these raw starting materials was >99%. The weighed starting reagents in appropriate ratios were milled in distilled water in a high-energy attrition mill (Szegvari Attritor System, Union Process, Ohio, USA) for 2 h, using zirconia media. The slurry was dried, sieved and then

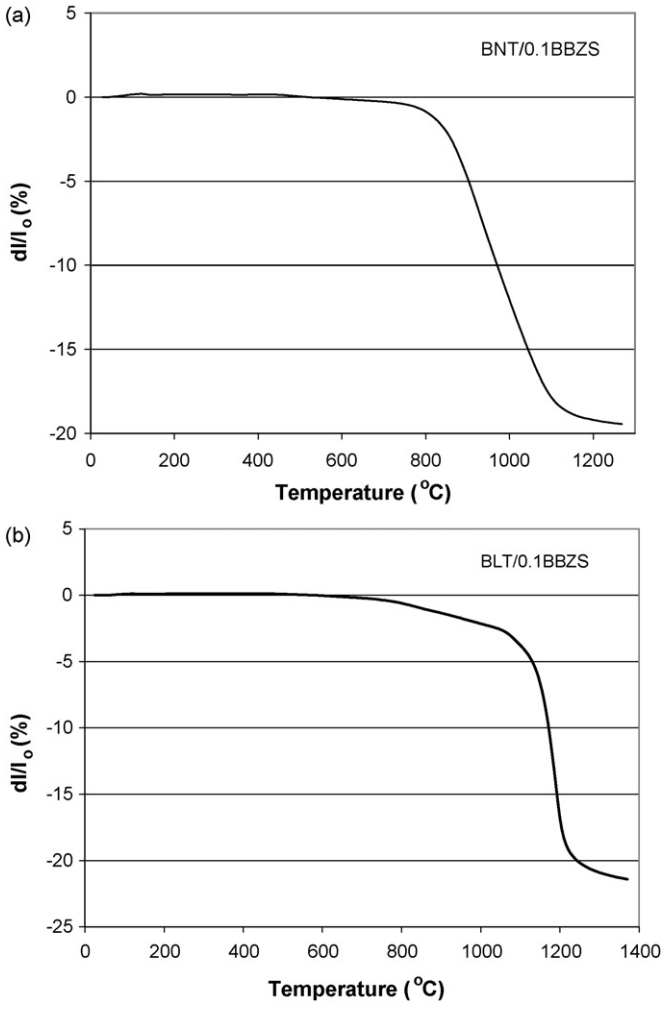

Fig. 2. Dilatometry data of (a) BNT/0.1BBZS and (b) BLT/0.1BBZS.

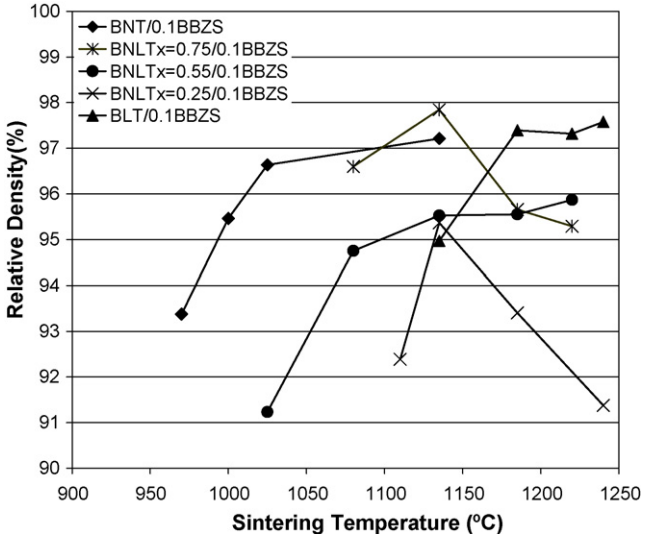

Fig. 1. Relative density as a function of sintering temperature in BNLT(xBNT − (1 − x)BLT)/0.1BBZS composite ceramics.

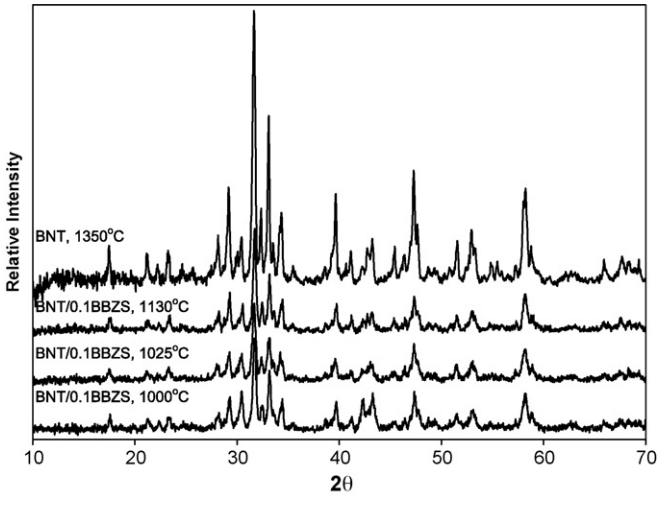

Fig. 3. XRD patterns obtained from BNT and BNT/0.1BBZS sintered at different temperatures.

calcined for 4–6 h at 1230 and 1100 °C for BLT and BNT, respectively. The calcined powders were then remilled and sieved. xBNT $-$ $(1-x)$BLT (BNLT) batches were obtained by mixing the BNT and BLT powders in appropriate molar ratios ($x = 0$, 0.25, 0.55, 0.75 and 1). The resultant BNLT composite powder was mixed with 10 wt% BBZS glass by ball-milling in distilled water for 18 h, and after drying and sieving, the mixture was pressed into discs and sintered 4 h between 950 and 1150 °C.

An X-ray diffractometer (Model PW 1730/10 Philips, Holland) with a Cu Kα source ($\lambda = 1.540562$ Å), operated at 40 kV and 30 mA, was used for the identification of crystal phases. A step size of 0.02°, a scan rate of 1°/min, and a scan range of 10–70° were adopted. Dilatometry data were collected using NETZSCH DIL 402 PC dilatometer (NETZSCH-Gerätebau GmbH, Wittelsbacherstrasse 42, 95100, Selb/Bavaria, Germany) with temperature range up to 1600 °C. The heating/cooling rate of the measurement was 3 °C/min.

A CAMSCAN scanning electron microscope (Series II, Cambridge, England), operating at 20 kV and equipped with an energy-dispersive spectroscope, was used to image the grain structures and to obtain qualitative compositional analyses.

Each sample for TEM was ground to approximately 20 μm thick after which a Cu support ring with an 800 μm circular hole was glued onto its surface. Samples were then thinned until perforation on a Gatan Duo Mill ion beam thinner operating at an accelerating voltage of 6 kV and a combined gun current of 0.6 mA at an incidence angle of 12–15°. TEM was carried out on an FEI Tecnai 20 operating at 200 kV equipped with EDS.

A Renishaw InVia Raman microscope was used for Raman measurements. This system comprised an integral Raman microscope, a stigmatic single spectrograph, a Peltier-cooled CCD detector and the excitation wavelength used was 514 nm. Power of 20 mW was incident on the samples in a 1–2 μm diameter spot through a standard 50× microscope objective lens. The spectra were collected with 10 s data point acquisition time, a spectral range of 150–950 cm^{-1} and a spectral resolution of ~2 cm^{-1}. Raman data were then analysed using WiRE^{TM} 2.0, which is a fully interactive data processing package including peak-fitting, data smoothing, quantitative analysis, peak picking and integration for Raman spectrum analysis. Spectra were presented as relative intensity (counts) versus Raman shift (wavenumber cm^{-1} in air).

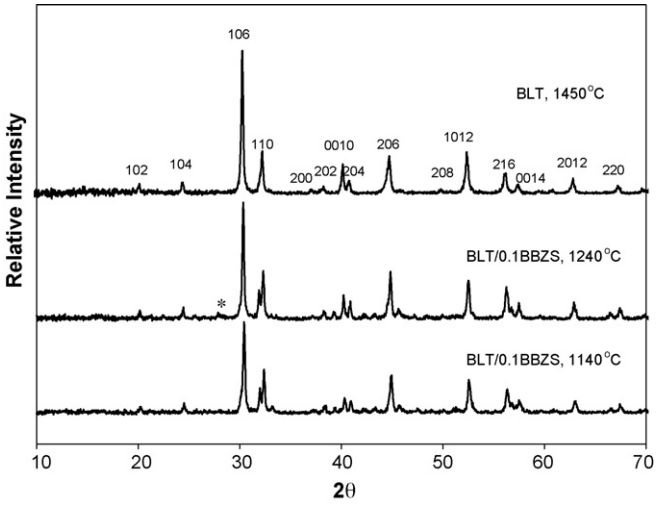

Fig. 4. XRD patterns obtained from BLT and BLT/0.1BBZS sintered at different temperatures.

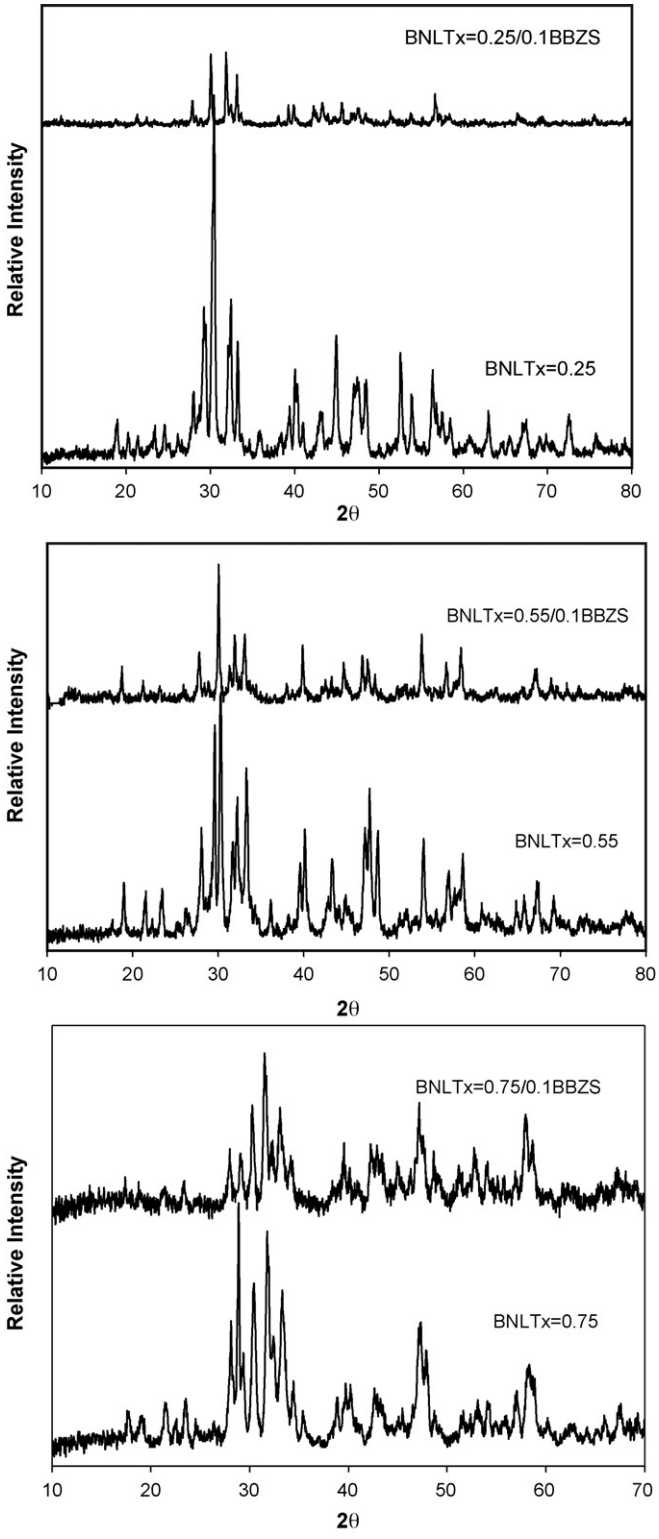

Fig. 5. XRD patterns obtained from BNLT and BNLT/0.1BBZS ($x = 0.25$, 0.55 and 0.75), respectively.

High-frequency microwave measurements (ε_r, Qf and τ_f) were performed using a silver-plated aluminium cavity and an Agilent vector network analyser (8753ES) with a range from 30 kHz to 6 GHz. Q is approximated using Eq. (1)

$$Q = \frac{f}{\mathrm{BW}}, \tag{1}$$

where f is the resonant frequency and BW is the bandwidth measured at 7 dB from the resonant peak minimum. τ_f measurements were performed in the same aluminium cavity placed inside a Tenney temperature control cabinet. Resonant frequency measurements were performed at 80, 20 and −20 °C, and τ_f was calculated using Eq. (2)

$$\tau_{\mathrm{f}} = \frac{(f_{80} - f_{-20})}{f_{20} \times 100}, \tag{2}$$

where f_{80} is the resonant frequency at 80 °C, f_{-20} is the resonant frequency at −20 °C and f_{20} is the resonant frequency at 20 °C.

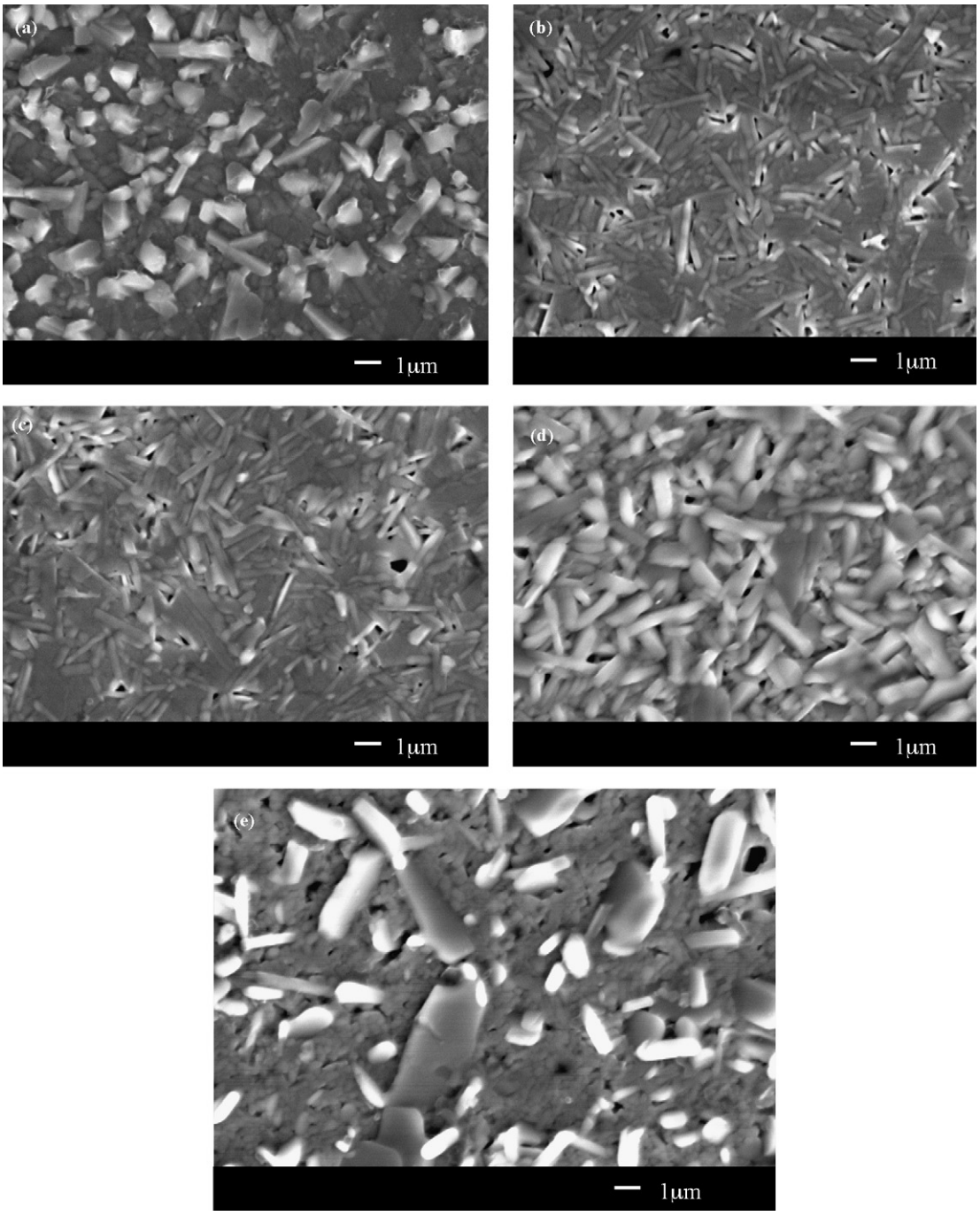

Fig. 6. SEI photographs of BNLT(xBNT − (1 − x)BLT)/0.1BBZS ceramics (a) $x = 0$, (b) $x = 0.25$, (c) $x = 0.55$, (d) $x = 0.75$ and (e) $x = 1$.

3. Results and discussion

3.1. Density measurement

The relative densities of BNT/0.1BBZS samples sintered at 1000 °C were >95% of theoretical, verifying that the sintering temperature of BNT ceramics (1350 °C[1]) was reduced by 350 °C with the addition of 10 wt% BBZS glass, Fig. 1. For BLT/0.1BBZS ceramics, relative densities ≥95% were achieved at ∼1140 °C, reducing the sintering temperature by 310 °C compared to pure BLT (1450 °C).[1] In comparison with BLT/0.1BBZS and BNT/0.1BBZS, relative densites ≥95% of theoretical for composite ceramics BNLT/0.1BBZS, $x = 0.25$, 0.55 and 0.75 were achieved by sintering at ∼1140 °C, a reduction of ∼310 °C in sintering temperature.[1] Although a decrease in densification was achieved through the glass addition, the discrepancy in the reduction in sintering temperatures between BLT/0.1BBZS and BNT/01.BBZS suggests that 10 wt% was insufficient to form a interconnected matrix of liquid phase throughout the composite during sintering.

3.2. Dilatometry

The dilatometry data of BNT/0.1BBZS in Fig. 2a revealed that shrinkage began at ∼600 °C, accelerated at ∼800 °C and was complete by ∼1100 °C. The total shrinkage from room temperature to 1300 °C was ∼19%. The maximum shrinkage rate occurred at ∼950 °C, which indicated that the densification could be achieved at ∼950 °C by introducing longer dwell times.

In contrast, BLT/0.1BBZS initially showed moderate shrinkage from 600 to 1000 °C, and then densified rapidly at ∼1000 °C, finally completing at ∼1280 °C, Fig. 2b. The total shrinkage of BLT/0.1BBZS was >20%. In general, the addition of 10 wt% BBZS glass to the BNT/BLT ceramics greatly reduced the onset temperature of densification. The discrepancies in the total shrinkage between BLT/0.1BBZS (>20%) and BNT/0.1BBZS (∼19%) may be explained by small variations in the green densities from sample to sample prior to dilatometry and by the formation of an unknown secondary phase, presumably of different density in BLT/0.1BBZS during the sintering. The different temperature regimes during which maximum shrinkage occurred in BLT/0.1BBZS (∼1000 °C) and BNT/01.BBZS (600–800 °C) supports the premise that, although BBZS acts as a sintering aid, 10 wt% is insufficient to form an interconnected liquid phase during sintering.

3.3. X-ray diffraction

The XRD patterns of BNT/0.1BBZS samples sintered between 1000 and 1130 °C are compared to those obtained from BNT, Fig. 3. No second phase peaks are apparent in the traces despite the addition of 10 wt% BBZS. Similarly, the XRD pattern of BLT/0.1BBZS samples sintered at 1140 °C are almost identical to that of BLT, Fig. 4. However, unidentified minor peak associated with secondary phase (marked * in the XRD pattern) appear in BLT/0.1BBZS samples sintered at higher temperatures. For xBNT − (1 − x)BLT composite ceramics with 10 wt% BBZS, XRD data show no evidence of any secondary phase compared to the respective xBNT − (1 − x)BLT composite ceramics within the XRD detection limit, Fig. 5.

3.4. SEM and EDS

The secondary electron images of BNLT/0.1BBZS ceramics, Fig. 6, revealed that in general, ceramics were dense with little porosity. Although some regions of brighter contrast are observed in the SEI images, in particular in BLT/0.1BBZS ($x = 0$, Fig. 6a) and BNT/0.1BBZS ($x = 1$, Fig. 6e), backscattered image (BEI), EDS (obtained from randomly selected grains, *A* and *B*) and dot mapping on BLT/0.1BBZS, Fig. 7, failed to differentiate any significant variation in elemental concentration from grain to grain. A more detailed TEM study was therefore performed, to further investigate the microstructure.

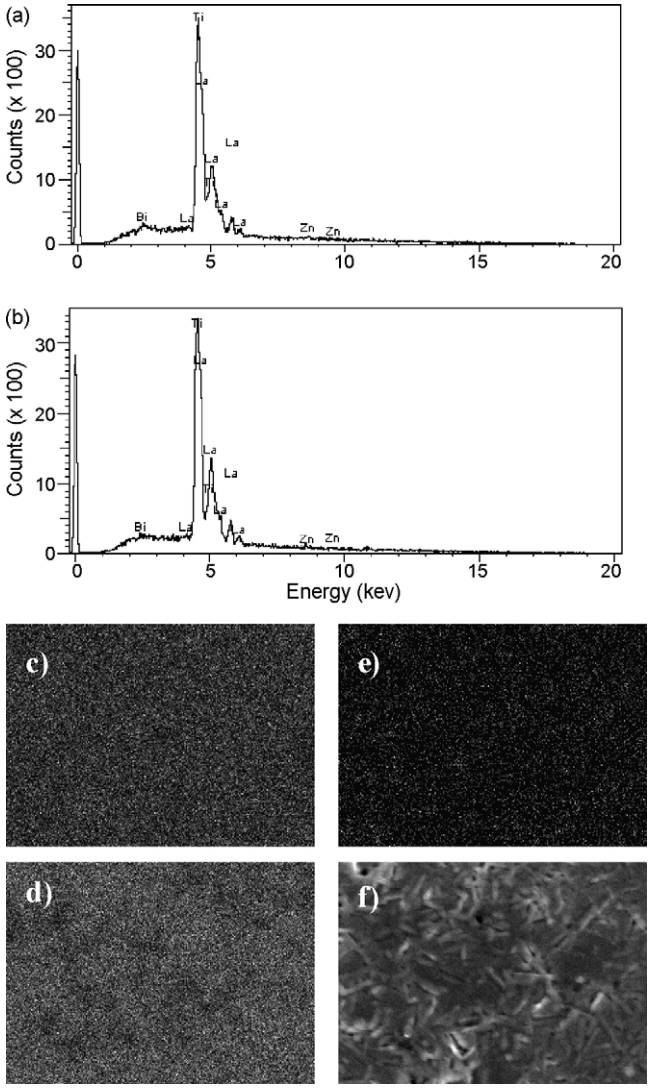

Fig. 7. EDS and mapping data of BLT/0.1BBZS ceramics: selective EDS spectra from (a) grain A and (b) grain B; distributions of element (c) La, (d) Ti, (e) Zn and (f) the corresponding dot mapping area shown by SEI image.

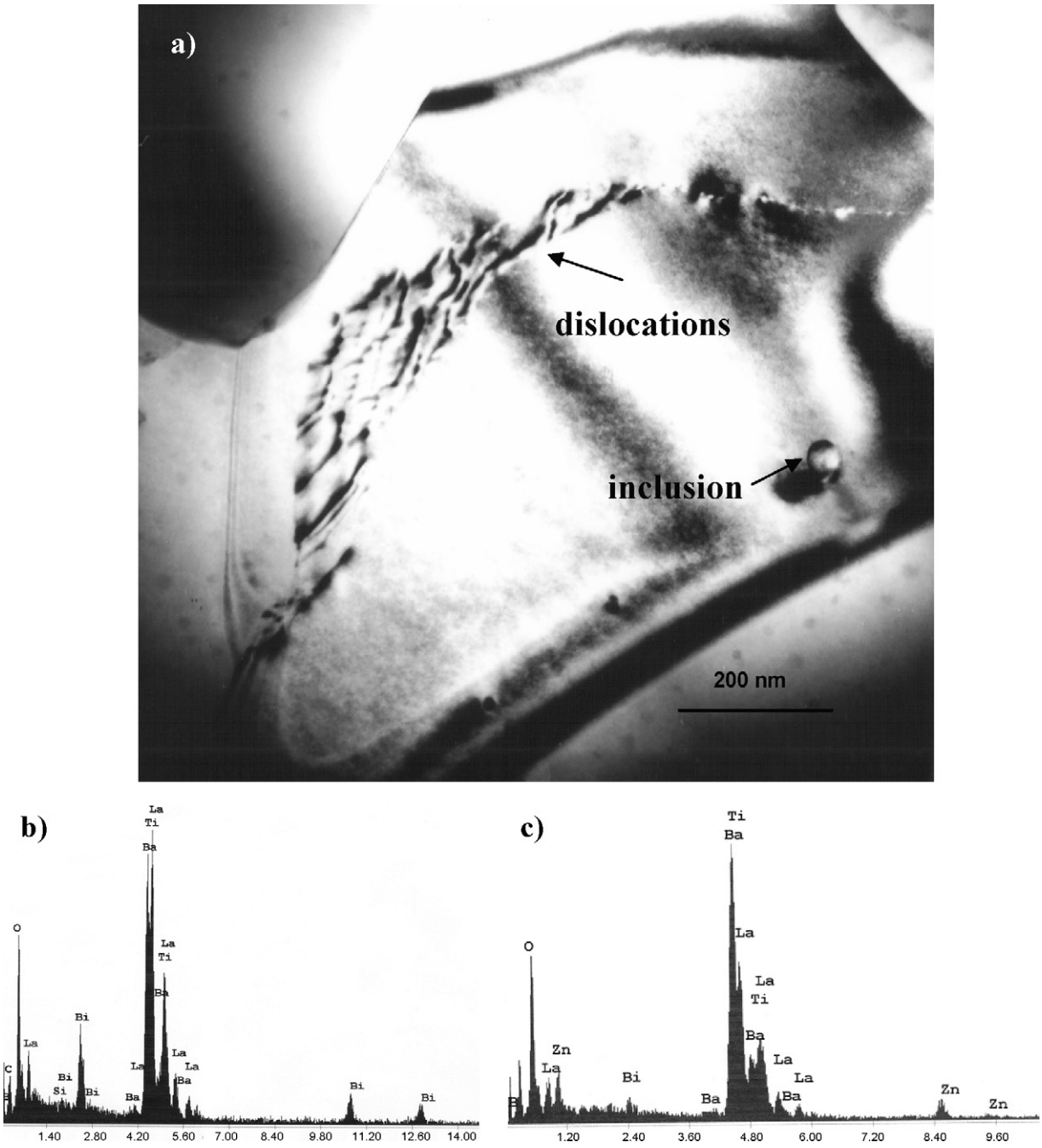

Fig. 8. (a) TEM image showing inclusions and dislocations in BLT/0.1BBZS ceramics, and EDS data obtained from (b) the inclusions and (c) dislocations.

3.5. TEM and EDS

Bright-field (BF) TEM images of BLT/0.1BBZS, Fig. 8a, revealed planar defects as well as inclusions present in the interior of BLT grains which are not present in BLT without glass addition. EDS revealed that the inclusion was rich in Bi and La (Fig. 8b) and the dislocation area usually contained some Zn (Fig. 8c), presumably as a result of the ceramic matrix reacting with the glass phase. In BNLT/0.1BBZS composites, residual glass was regularly observed at the grain boundary triple junctions, as exemplified by the BF TEM image obtained from BNLT/0.1BBZS ($x = 0.75$), Fig. 9a. According to EDS, Fig. 9b, the residual glass phase was rich in Zn, Bi, Si and B glass elements. In addition, in this composition, BNT grains coexisted with BLT, Fig. 9a, and were readily distinguished since the BLT grains were lath-shaped ($\sim 1\,\mu m \times 0.5\,\mu m$) whereas the BNT grains were equiaxed (~ 250 nm).

3.6. Raman spectroscopy

Compared to BLT, Fig. 10a, the Raman spectra obtained from BLT/0.1BBZS exhibit similar numbers of Raman-active modes. Moreover, the position of the bands is almost identical, suggesting that no additional second phase/lowering of symmetry has

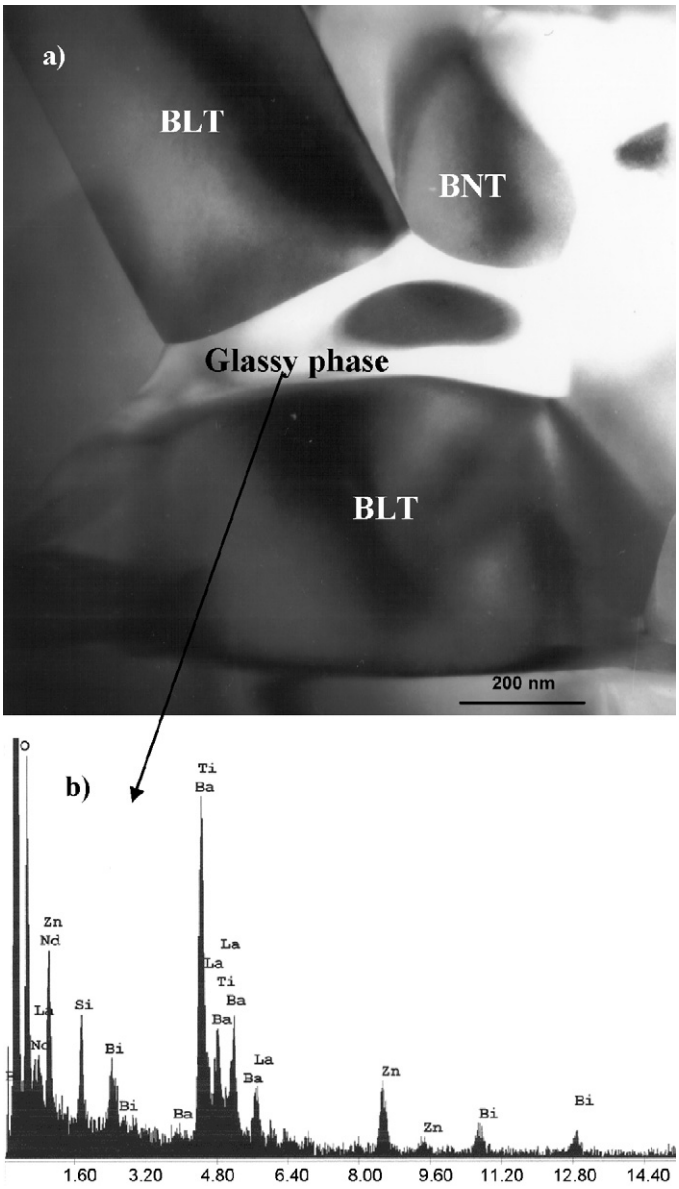

Fig. 9. (a) TEM image showing glassy phase in BNLT/0.1BBZS ($x = 0.75$) and (b) EDS data obtained from the glassy phase.

occurred as a result of adding BBZS to BLT ceramics. However, each corresponding peak is broadened for the BBZS glass doped samples. In general broadening of peaks in techniques such as Raman spectroscopy and XRD diffraction indicate a smaller effective crystallite size. The effective crystallite size is not necessarily the same as the particle or grain size but may also be reduced by planar and lattice defects. The presence of dislocations and inclusions in the matrix phase and evidence of reaction between the BLT and BBZS glass in BLT/0.1BBZS (Fig. 8a), supports this premise. BNT/0.1BBZS exhibits a similar spectrum to BNT but there are some weak extra modes particularly at high wavenumbers (arrowed) which may arise from phases other than BNT, Fig. 10b. The cause of these extra modes is uncertain.

In the 10 wt% BBZS glass-added BNLT compositions, Fig. 11, extra Raman peaks are observed at ~310 and ~880 cm^{-1} that are not present in other spectra. Their absence

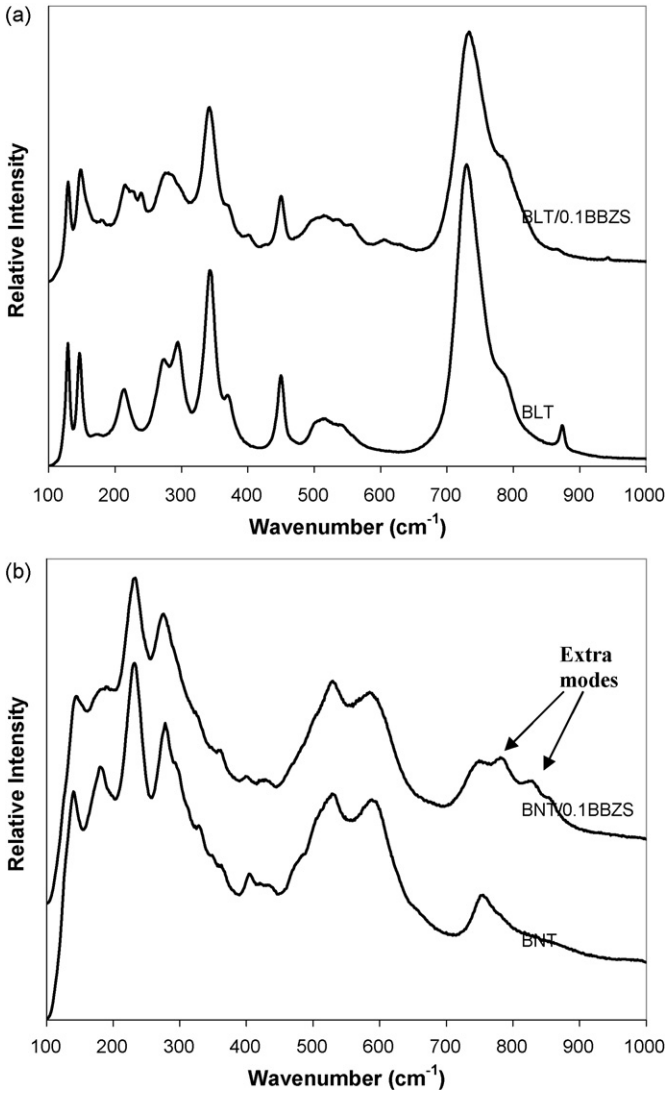

Fig. 10. Raman spectra from (a) BLT vs. BLT/0.1BBZS and (b) BNT vs. BNT/0.1BBZS.

in BLT/0.1BBZS and BNT/0.1BBZS and the fact that they are strongest and narrowest in the $x = 0.55$ composition and occur irrespective of whether BBZS is added, suggests that they form as a result of the interaction of BLT and BNT only. It is suspected that these two bands may be of the similar nature to the B-site order–disorder bands observed in complex or solid solution perovskites as reported[9–11] due to the La/Nd cations occupying the similar sites; however it is also possible that these two bands arise from second phases present in the intermediate compositions as discussed in previous work.[1]

3.7. Microwave properties

Fig. 12 reveals that the ε_r of BNT/0.1BBZS ceramics is ~71, compared with BNT, $\varepsilon_r = 78$.[1] In contrast, the ε_r of BLT/0.1BBZS ceramics is ~47, which is increased compared to BLT, $\varepsilon_r = 45$.[1] This further suggests that reaction has occurred between the BBZS glass and BLT and is consistent with the presence of second phase peaks in the XRD data. The τ_f val-

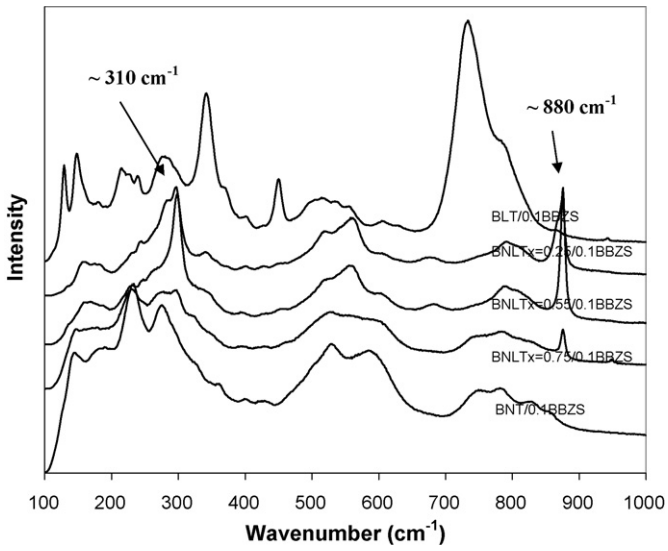

Fig. 11. Raman spectra obtained from BNLT(xBNT − (1 − x)BLT)/0.1BBZS ($0 \le x \le 1$).

ues of BNT/0.1BBZS and BLT/0.1BBZS are −3 and 3 ppm/°C, respectively, in comparison with BNT ($\tau_f \sim 47$ ppm/°C[1]) and BLT ($\tau_f \sim -2$ ppm/°C[1]), Fig. 12. For intermediate compositions, ε_r decreases to 43 for $x = 0.25$ before increasing linearly with x. In contrast, τ_f increases to 60 ppm/°C for $x = 0.25$ before decreasing. These non-systematic variation suggest that there is interaction between the BNT, BLT and BBZS glass. Similarly, Qf varies in a non-systematic manner, achieving a maximum for BLT/0.1BBZS and BLNT/0.1BBZS ($x = 0.75$), Fig. 13. Qf is a minimum (800 GHz) for $x = 1$, strongly contradicting the value of 6000 GHz reported by Dernovsek et al.[3] At the present time, there is no rationalisation for the discrepancy between the work reported here and that of Dernovsek et al.[3]

The MW properties generally appear promising for LTCC and antenna core applications, in which high permittivity $47 \le \varepsilon_r \le 67$, low τ_f and moderate Qf values are required in combination with low sintering temperatures. Although further work may be required to improve Qf to >3000 GHz.

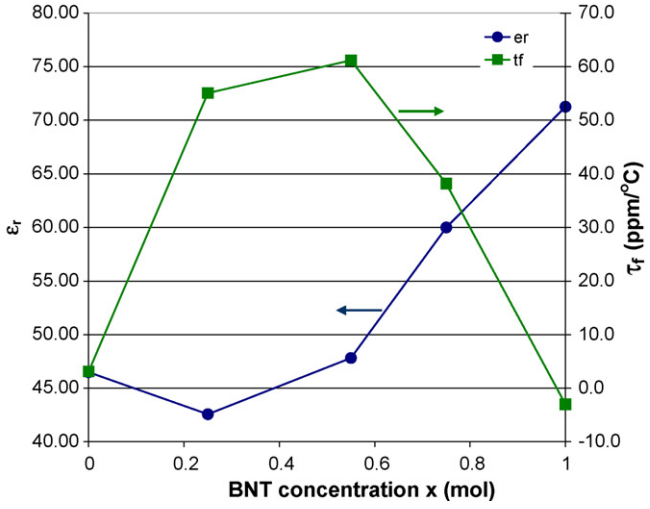

Fig. 12. ε_r and τ_f as a function of x in BNLT(xBNT − (1 − x)BLT)/0.1BBZS ($0 \le x \le 1$).

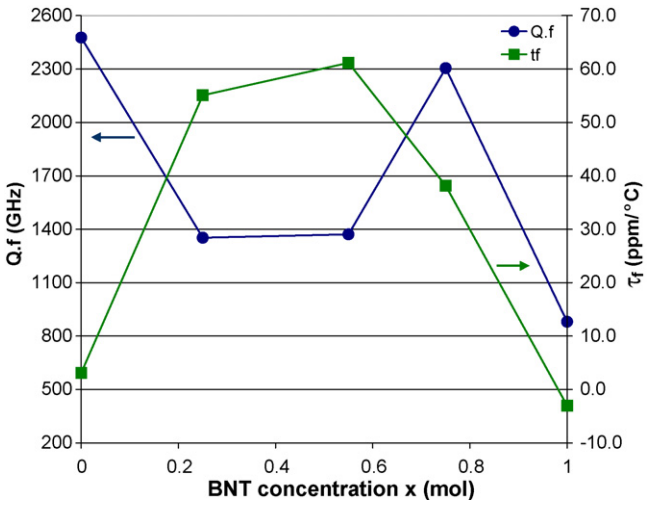

Fig. 13. Qf and τ_f as a function of x in BNLT(xBNT − (1 − x)BLT)/0.1BBZS ($0 \le x \le 1$).

4. Conclusions

- The addition of 10 wt% BBZS glass in BNLT ceramics lowers the sintering temperature by 310–350 °C to temperatures between 950 and 1140 °C, depending on composition x.
- No second phase peaks are observed by XRD in BNLT/0.1BBZS and although some bright regions of contrast were observed by SEM.
- TEM studies revealed the presence of Zn-contained dislocations and Bi-rich inclusions as well as a glassy phase rich in Bi, Zn, B and Si often observed at grain triple-junction, in BNLT/BBZS.
- The addition of BBZS glass to BNLT has negligible effect on ε_r and τ_f microwave properties, however the Qf is significantly deteriorated in BNLT/BBZS composites.
- The optimised composition (xBNT − (1 − x)BLT)/0.1BBZS ($x = 0.75$) has $\varepsilon_r \sim 61$, $\tau_f \sim 38$ ppm/°C and $Qf \sim 2305$GHz.

References

1. Zheng, H., Reaney, I. M., Muir, D., Price, T. and Iddles, D. M., Composite dielectric ceramics based on BaO–Ln_2O_3–TiO_2 (Ln = Nd, La). *Jpn. J. Appl. Phys.*, 2005, **44**, 3087–3090.
2. Yanchevskii, O. Z., V'yunov, O. I. and Belous, A. G., Fabrication and properties of semiconducting barium lead titanate ceramics containing low-melting glass additions. *Inorg. Mater.*, 2003, **39**, 645–651.
3. Dernovsek, O., Naeini, A., Preu, G., Wersing, W., Eberstein, M. and Schiller, W. A., LTCC glass-ceramic composites for microwave application. *J. Euro. Ceram. Soc.*, 2001, **21**, 1693–1697.
4. Zhang, B., Yao, X. and Zhang, L., Study on the structure and dielectric properties of BaO–SiO_2–B_2O_3 glass-doped (Ba,Sr)TiO_3 ceramics. *Ceram. Inter.*, 2004, **30**, 1767–1771.
5. Cheng, C. C., Hsieh, T. E. and Lin, I. N., Microwave dielectric properties of glass-ceramic composites for low temperature co-firable ceramics. *J. Euro. Ceram. Soc.*, 2003, **23**, 2553–2558.
6. Cho, I. S., Kim, D. W., Kim, J. R. and Hong, K. S., Low-temperature sintering and microwave dielectric properties of $BaO{\cdot}(Nd_{1-x}Bi_x)_2O_3{\cdot}4TiO_2$ by the glass additions. *Ceram. Inter.*, 2004, **30**, 1181–1185.
7. Chang, L. C., Chiou, B. S. and Lee, W. H., Effect of glass additions on the sintering behaviours and electrical microwave properties of

$BaO–Nd_2O_3–Sm_2O_3–TiO_2$ ceramics. *J. Mater. Sci.: Mater. Electron.*, 2004, **15**, 153–158.

8. Takada, T., Wang, S. F., Yoshikawa, S., Jang, S. J. and Newnham, R. E., Effect of glass additions on $BaO–TiO_2–WO_3$ microwave ceramics. *J. Am. Ceram. Soc.*, 1994, **77**, 1909–1916.
9. Zheng, H., Reaney, I. M., Ubic, R., Yarwood, J., Seabre, P. and Ferreira, V., Raman spectroscopy of $CaTiO_3$-based perovskite solid solutions. *J. Mater. Res.*, 2004, **19**, 488–495.
10. Zheng, H., Bagshaw, H., Csete de Györgyfalva, G. D. C., Reaney, I. M., Ubic, R. and Yarwood, J., Raman spectroscopy and microwave properties of CaTiO3-based microwave ceramics. *J. Appl. Phys.*, 2003, **94**, 2948–2956.
11. Zheng, H., Csete de Györgyfalva, G. D. C., Quimby, R., Bagshaw, H., Ubic, R., Reaney, I. M. and Yarwood, J., Raman spectroscopy of B-site order–disorder in $CaTiO_3$-based microwave ceramics. *J. Euro. Ceram. Soc.*, 2003, **23**, 2653–2659.